Ceramics International 42 (2016) 17482–17488

Contents lists available at ScienceDirect

Ceramics International

journal homepage: www.elsevier.com/locate/ceramint

Influence of spark plasma consolidation conditions on the superconducting properties of (Bi,Pb)-Sr-Ca-Cu-O ceramic samples

F. Rosales-Saiz [a], L. Pérez-Acosta [b], I.F. Machado [c], J.E. Pérez-Fernández [d], R.F. Jardim [e], E. Govea-Alcaide [a,*]

[a] Departamento de Matemática-Física, Facultad de Ciencias Informáticas, Naturales y Exactas, Universidad de Granma, Apdo. 21, P. O. Box 85100, Bayamo, Cuba
[b] Departamento de Física, Facultad de Electromecánica, Universidad de Camagüey, Circunvalación Norte Km 5 1/2s/n, Camagüey, Cuba
[c] Departamento de Engenharia Mecatrônica e Sistemas Mecânicos, Escola Politécnica, Universidade de São Paulo, 05508-900 São Paulo, SP, Brazil
[d] Departamento de Ingeniería Mecánica, Facultad de Ciencias Técnicas, Universidad de Granma, Apdo. 21, P. O. Box 85100, Bayamo, Cuba
[e] Instituto de Física, Universidade de São Paulo, Rua do Matão, 1371, CEP 05508-090 São Paulo, SP, Brazil

ARTICLE INFO

Article history:
Received 4 July 2016
Received in revised form
3 August 2016
Accepted 8 August 2016
Available online 9 August 2016

Keywords:
Bi-based superconductor
Spark plasma sintering
Finite element method
Superconducting properties

ABSTRACT

The influence of different plungers/die materials for the synthesis of (Bi, Pb)$_2$ $Sr_2Ca_2Cu_3O_{10+\delta}$ (Bi-2223) superconductors via the spark plasma sintering SPS method and by using two different setups made of all-graphite and all-steel were investigated. AISI H13 die steel, which is widely used as a hot forging die, was chosen to verify the methodology. In the all-steel setup, samples were consolidated at 700 and 750 °C, for 5 min, and subjected to two different heating rates of 135 and 50 °C/min. Moreover, by using the all-graphite setup, a sample was consolidated at 750 °C, for 5 min by using a heating rate of 145 °C/min. Irrespective of the type of plungers/die materials used, the X-ray diffraction analysis indicate the occurrence of an extra phase $Bi_2Sr_2CaCu_2O_{8+\delta}$ (Bi-2212) in all samples and its volume fraction was estimated to be comprehended between ~3% and 60%. In samples consolidated with the all-steel setup at 750 °C, for 5 min, and a heating rate of 50 °C/min, the volume fraction of the Bi-2212 phase was found to be as high as 60%. Computational simulations, by using the Finite Element Method (FEM) with an integrated PID control, were performed to evaluate the temperature profile within samples during the SPS consolidation. The model was then validated by comparing its predictions with experimental results, showing good agreement. From the temperature dependence of magnetization $M(T)$, performed in powder and pellet samples, we have inferred that superconductivity arises from grains with core-shell morphology, where the shell is oxygen deficient. The influence of carbon contamination as the mechanism responsible for the oxygen deficiency in SPS samples has been considered and refuted by the current data. No evidence of the role played by the carbon contamination or reduction in promoting the formation of grains with core-shell morphology has been found. We also argue that the consolidation process, conducted under vacuum, is responsible for the origin of an oxygen deficiency shell near grain boundaries in Bi-2223 samples.

1. Introduction

The spark plasma sintering (SPS) method has received much attention in the last decade because it provides the synthesis of many materials at relatively low temperatures, within a brief time interval of a few minutes, and with an adequate control of size and size distribution of grains [1,2]. In the SPS process the densification of a powder sample is promoted by the simultaneous action of a uniaxial compacting pressure and a high direct electric current [1]. The use of SPS to consolidate cuprate superconductors is a difficult task because the process is performed under vacuum and the general transport properties of these superconducting materials are very sensitive to their oxygen content [3]. In $Bi_{1.65}Pb_{0.35}Sr_2Ca_2Cu_3O_{10+\delta}$ (Bi-2223) samples, the SPS consolidation is responsible for a deoxygenation near grain boundaries of ceramic samples. The obtained pellets are comprised of grains with a shell-core morphology in which the shell is oxygen deficient and strongly dependent of the consolidation temperature, T_D, used during the SPS process, e.g., the higher is T_D, the higher is the width of the oxygen deficiency shell of the grains [4,5]. As a consequence, consolidated samples of Bi-2223 by the SPS technique exhibit very low superconducting critical current density at 77 K,

* Corresponding author.
E-mail address: egoveaa@udg.co.cu (E. Govea-Alcaide).

http://dx.doi.org/10.1016/j.ceramint.2016.08.053
0272-8842/

J_c($\leq$ 50 A/cm^2) [4]. In order to restore the oxygen content of the materials processed by the SPS method, many authors have used a post-annealing heat treatment (PAHT) to re-oxygenate the samples and therefore to improve the desirable properties of the materials [4–8].

Usually, the spark plasma sintering process is conducted by using a setup built with high-density graphite die and plungers, denominated here of all-graphite setup (A-GS) [9]. The A-GS setup has some disadvantages associated with its thermal and mechanical properties [9]. For instance, barium ferrite materials obtained by using the A-GS set up exhibit carbon contamination and reduction of Fe^{3+} to Fe^{2+}, due to the diffusion of carbon monoxide within the samples [10]. More recently, Mackie et al. have demonstrated the carbon uptake by samples of Sm(Co, Fe, Cu, Zr)$_z$ obtained by the SPS method [11], as inferred from carbon distribution maps of the samples obtained by using Electron Probe Micro-Analysis (EPMA). The results indicate a carbon contamination within the samples, a feature especially pronounced at the surface of the materials. Such undesired results may be minimized by replacing graphite for others materials. As far as this point is concerned, the use of steel has been proposed in order to reduce the electrothermal loss during the SPS process, a mechanism known as reduced electrothermal loss SPS (RETL-SPS) [9]. Nevertheless, the use of an all-steel setup to consolidate Bi-2223 superconductors is absent in the literature.

Within this context, we describe here an investigation on the influence of the material die and plungers on the superconducting properties of $Bi_{1.65}Pb_{0.35}Sr_2Ca_2$ $Cu_3O_{10+\delta}$ samples processed by the spark plasma sintering method. Samples were then consolidated by using two setups comprised of different materials: all-steel and all-graphite. Finite element simulations (FEM) were performed to provide extra information regarding the distribution of temperature within the samples. X-ray diffraction (XRD) analysis and DC magnetization as a function of temperature, $M(T)$, have been conducted in all synthesized samples as complementary characterizations. The main motivation of this study is to evaluate the influence of the material setup of the SPS apparatus on the deoxygenation of Bi-2223 compounds consolidated by the SPS method.

2. Experimental procedure

Nearly single-phase powders of $Bi_{1.65}Pb_{0.35}Sr_2Ca_2Cu_3O_{10+\delta}$ (Bi-2223) were prepared by mixing appropriate amounts of Bi_2O_3, PbO, $SrCO_3$, $CaCO_3$, and CuO, in an atomic ratio of Pb: Bi:Sr: Ca:Cu (0.35:1.65:2:2:3). The mixture was first calcined in air atmosphere at 750 °C for 40 h. Then, the powder was reground and pressed into pellets of 20 mm in diameter and 2 mm in thickness at a pressure of 250 MPa. These pellets were heat treated at 800 °C in air for 40 h. Subsequently, the samples were reground, pressed again, and sintered in air at 845 °C for 40 h. This step was repeated three times. The obtained pellets were reground again and the resulting pre-reacted powder was used to be consolidated by spark plasma sintering.

The final consolidation of the samples was performed in an SPS 1050 Dr Sinter® apparatus. Two types of materials for plungers/die were used to consolidate the pre-reacted powders of Bi-2223, thereafter referred to as pristine powder: (i) the AISI H13 steel; and (ii) a high-density graphite. Once the powder was placed within the die, then all setup was situated inside the chamber of the SPS apparatus [4]. The sintering was performed under vacuum (roughly from 10 to ~30 Pa) and a uniaxial pressure along the z-axis of 50 MPa. The identification of the SPS consolidated samples, where H and G stand for those synthesized by using the all-steel and all-graphite setups, respectively, as well as the parameters used during their synthesis are displayed in Table 1. The

Table 1
Consolidation parameters used during the SPS process for producing Bi-2223 samples. T_D is the consolidation temperature, HR is the heating rate, t_r is the heating time, and t_D is the consolidation time. We also included values of the density of the pellets, D.

Sample	T_D (°C)	HR (°C/min)	t_r (min)	t_D (min)	D (g/cm^3)
H1	700	135	5	5	4.8
H2	750	50	15	5	5.5
G1	750	145	5	5	5.7

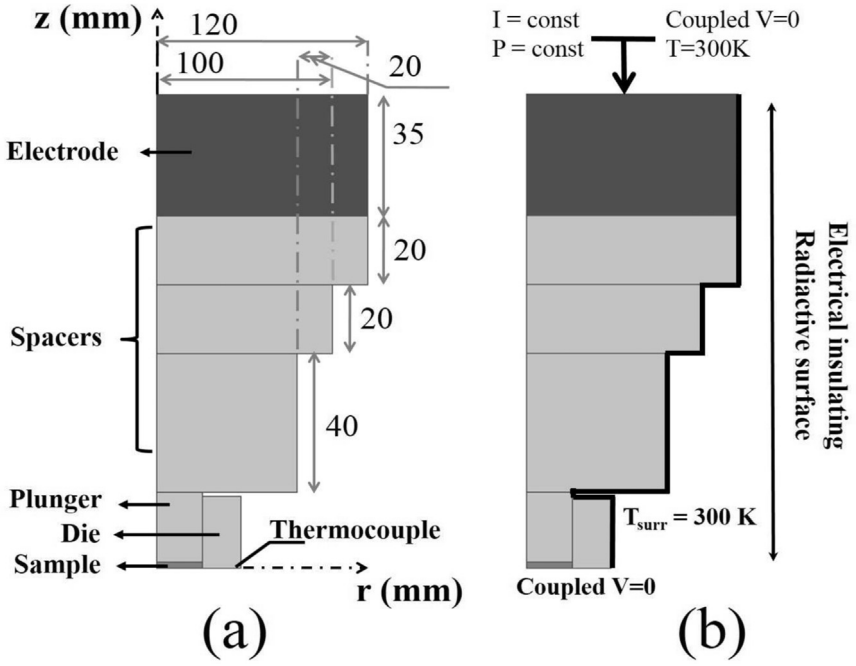

Fig. 1. (a) Schematic drawing of the consolidation system; (b) boundary conditions.

relevant parameters are the consolidation temperature, T_D, the heating rate, HR, the heating time, t_r, and the consolidation time t_D. The temperature was measured and controlled during the consolidation process by using a (K-type) thermocouple located in a small hole at 3 mm from the outer surface of the die (see Fig. 1 (a)). After the sintering process, each sample was first allowed to cool naturally for about 50 min and then removed from the die. In order to restore the oxygen content of the consolidated samples, they were subjected to a post-annealing heat treatment PAHT performed in air, at 750 °C for 5 min. These samples are thereafter refereed to as H1+O_2, H2+O_2, and G1+O_2, following a similar notation above described.

The phase identification of the samples was evaluated, in both powder and pellet samples, by means of X-ray diffraction (XRD) patterns obtained in a Bruker-AXS D8 Advance diffractometer at room temperature. These measurements were performed using Cu Kα radiation in the $3 \leq 2\theta \leq 80°$ range with a 0.05° (2θ) step size, and 5 s counting time. The density of all pellets, D, was determined by the Archimedes method.

DC magnetization measurements were performed in a commercial SQUID magnetometer from Quantum Design in pellet and powder samples. The temperature dependence of the magnetization, M(T), was measured under both zero-field-cooled (ZFC) and field-cooled (FC) conditions. The ZFC cycle was performed after cooling down the sample to 10 K without the application of any magnetic field. After this step, a small measuring magnetic field $H=5$ mT is applied, and the M(T) data collected by increasing the temperature from 10 K to 150 K. Subsequently, the FC measurements were performed after the ZFC cycle. The samples were cooled slowly from 150 K down to 10 K in the same applied magnetic field of 5 mT and the magnetization data recorded during the cooling process.

3. Finite element method simulations

The SPS setup used for processing our samples does not allow simultaneous measurements of temperature and electric current intensity. For this reason, is necessary to follow a specific procedure in order to determine the values of these parameters. As the finite element method FEM in SPS electro-thermal problem model is a powerful tool for comparing experimental and theoretical of SPS processes, it has been employed here for our analysis [12]. The arrangement consist of two Inconel electrodes, six graphite spacers, the die (thickness 11 mm, height 21 mm) with two plungers (diameter 26 mm, height 20 mm) surrounding the sample (diameter 26 mm, height 2 mm), the latter located in the center of the stack. Taking into account the axisymmetrical configuration, only two dimensions are of the interest: the system is studied in cylindrical coordinates and the problem is rather simplified. The schematic drawing of the consolidation system and boundary conditions are displayed in Fig. 1. For each one of the above domains, the electro-thermal process is described by a two coupled partial differential equations: one related to the charge conservation law and the other one associated with the heat transfer process by itself [2,13]

$$\nabla \cdot J = \nabla \cdot (\sigma E) = \nabla \cdot (-\sigma \nabla V) = 0, \tag{1}$$

$$\rho c_p(T) \partial T / \partial t - \nabla \cdot (k \nabla T) = \dot{q}_J. \tag{2}$$

where T is the temperature, ρ is the density, assumed constant and corresponding to the last stage of sintering, $\dot{q}_J = JE$ is the heat loss by Joule heating per unit volume per unit time, $J = E/\rho_e(T)$ is the electric current density, $\rho_e(T)$ is the temperature dependence of the electrical resistivity, $c_p(T)$ is the heat capacity as a function of temperature, and $k(T)$ is the thermal conductivity. Values for each parameter are assigned for each material or domain in the geometry, i.e., the Inconel 600, the high-density graphite, the AISI H13 steel, and the Bi-2223 sample. Table 2 displays the parameters used in the FEM simulations.

The initial and boundary conditions used for solving Eqs. (1) and (2) are displayed in Fig. 1(b). The initial temperature was set to be 300 K and the heat losses by conduction and/or convection through the gas were neglected because the process occurs in a vacuum. All the free surfaces exposed to the vacuum chamber have heat losses by radiation and are given by $\dot{q}_{rad} = \sigma_s \varepsilon (T_d^4 - T_0^4)$, where T_d is the temperature of the free surfaces, σ_s the Stefan-Boltzmann's constant, $\varepsilon=0.3$ (0.69) is the graphite (Inconel 600) emissivity, and $T_0=300$ K is the temperature of the wall chamber. The temperature of both the upper and lower Inconel electrodes was 300 K and the electrical and thermal resistances were disregarded [2]. A preset time-current profile $I(t)$ is directly applied on the top of the electrode. Finally, the electro-thermal Eqs. (1) and (2) were solved by using the COMSOL Multiphysics™ package.

There are two forms for controlling the SPS process: (i) temperature control; and (ii) current intensity control. In our simulations, the former has been employed, i.e., a preset time-current profile $I(t)$ is directly applied as a function of the measured temperature in a close-loop control system in such a way that a preset time-temperature $T(t)$ profile is reached. A proportional-integral-derivative (PID) control has been programmed into the COMSOL code. The current profile $I(t)$ is given by

$$I(t) = k_P e(t) + k_I \int_0^t e(t)dt + k_D (de(t)/dt), \tag{3}$$

where $e(t)$ is the difference between the desired temperature and the actual temperature of the control point. Values of k_P, k_I, and k_D are then obtained by adjusting the PID control with the Ziegler-Nichols method [15].

4. Results and discussion

Table 1 displays the identification of the samples according to their consolidation conditions. In addition, the temperature profiles of samples H1, H2, and G1 are shown in Fig. 2. In all cases, the temperature at the position of the thermocouple increases as the processing time is increased. For samples H1 and H2 (see Fig. 2 (a) and (b), respectively) the temperature increases non-linearly during the heating, $t \leq t_r$, in contrast to the linear behavior observed in the profile of sample G1 (Fig. 2 (c)). During the consolidation time, $t_r \leq t \leq t_D$ (see insets of Fig. 2), there is a small, but perceptible difference between the experimental temperature profiles. In sample H1 (Fig. 2(a)), when the sintering time attains t_D, the PID temperature controller of the SPS machine hardly stabilizes the system, i.e., the temperature oscillates between ± 25 °C in the vicinity of $T_D = 725$ °C. This behavior may be ascribed to a combination of physical properties of the AISI H13 steel, e.g., electrical resistivity and thermal conductivity, as discussed below.

A possible way to minimize the overheating observed in the temperature profile of sample H1 is decreasing the heating rate or, equivalently, to increase the heating time. These changes were made, resulting in sample H2, and its temperature profile is displayed in Fig. 2(b). For this particular case, the obtained results are of interest. We first mention that the temperature measured at the position of the thermocouple increases nonlinearly, reaching a plateau at $T \sim 725$ °C for $t \geq 8$ min. At $t = t_r = 15$ min (see Table 1), the temperature starts to oscillate in a range of ± 25 °C close to $T_D = 750$ °C. On the other hand, when the all-graphite setup is

Table 2
Parameters of Bi-2223 samples, graphite, Inconel 600, and the H13 steel used in the FEM simulations: ρ is its density, $\rho_e(T)$ is the electrical resistivity as a function of temperature, $c_p(T)$ is the heat capacity as a function of temperature, and $k(T)$ is the thermal conductivity.

Physical property	Bi-2223	High-density graphite	Inconel 600	AISI H13	Units
ρ	5700*	1900	8175	7670	kg/m^3
$\rho_e(T)$	$0.8 \times 10^{-6} + 0.8 \times 10^{-8}T$	$2.4 \times 10^{-5} - 2.6 \times 10^{-8}T + 2.2 \times 10^{-11}T^2$	$1.03 \times 10^{-6} - 1.85 \times 10^{-10}T + 6.2 \times 10^{-13}T^2$	$4.3 \times 10^{-7} + 1.7 \times 10^{-10}T + 5 \times 10^{-13}T^2$	Ω m
$c_p(T)$	$131.6 + 0.77T$	$-151 + 2.3T - 7.1 \times 10^{-4}T^2$	$395.28 + 0.1576T + 7.1 \times 10^{-5}T^2$	$488.044 - 0.2T + 3 \times 10^{-4}T^2$	J/kg K
$k(T)$	$0.27 + 1.95 \times 10^{-3}T$	$84 - 0.063 \times T + 2.9 \times 10^{-5} \times T^2$	$8.955 + 0.016T$	$-11.36 + 0.15T$	W/m K

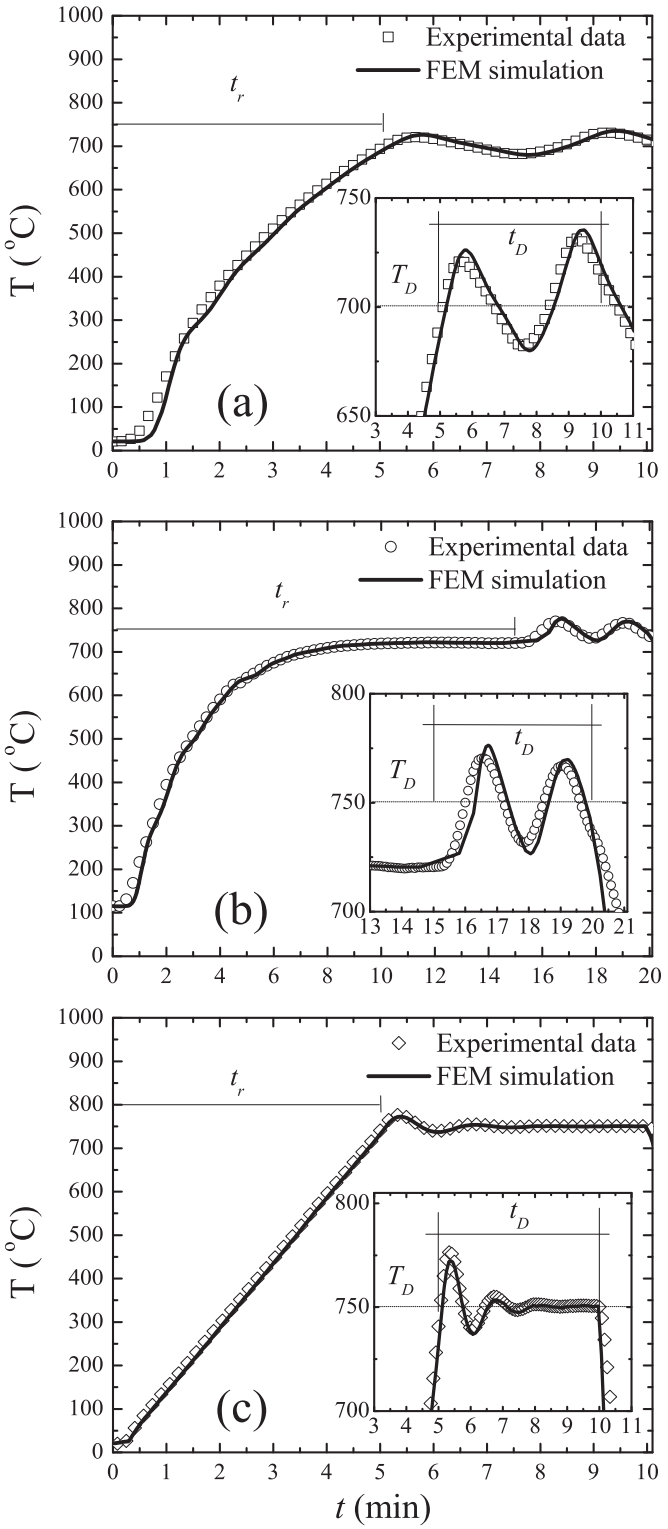

Fig. 2. Temperature profile during the SPS consolidation of samples H1 (a), H2 (b), and G1 (c). The sintering conditions for the synthesis of the three samples are displayed in Table 1. The inset displays an expanded view of the consolidation region. Solid lines represent the profile fittings by using FEM simulations (see text for details).

used, the consolidation of the sample G1 occurs according to the predefined conditions (see Table 1). As observed in Fig. 2(c), the temperature increases linearly and reaches a maximum of 775 °C during the time interval of the consolidation process. In this case,

the PID controller stabilized well and the consolidation temperature of $T_D = 750$ °C varied little, between $7 \le t \le t_D$. The finite element method simulations were performed for the SPS consolidation processes by using all-steel and/or all-graphite setups. Before any analysis, it is important to notice that the first step here is to validate the model presented in Section 3, by comparing its predictions with the experimental temperature profile data. Figs. 2 (a)–(c) show the correspondence between the experimental temperature profiles (scatter symbols) and results from the FEM simulations (solid lines). We note here that our FEM simulations, as well as in the real sintering processes, were carried out by controlling the temperature at the thermocouple position ($r = 21$ mm, $z=0$). As observed, there is a very good agreement between the experimental data and the FEM simulations, a feature that gives a good level of reliability to the model for the consolidation of the pre-reacted powders of Bi-2223 by the SPS method.

Based on previous results, we are now able to perform a critical analysis of the consolidation process. Fig. 3(a) displays the simulated temperature difference profiles, $|\Delta T(t)|$, between the center ($r=0$; $z=0$) and the thermocouple ($r = 21$ mm; $z=0$) during the spark plasma sintering of samples H1, H2, and G1. The most relevant information of these curves is related to the behavior of $|\Delta T(t)|$ during the time interval $(t_r \le t \le t_D)$ in which the consolidation process takes place. In samples obtained by using the all-steel setup, the difference in the estimated temperatures is appreciable. Results indicate that, in sample H1, the difference in the average temperature is $\overline{|\Delta T|} = (37 \pm 3)$°C, and that $|\Delta T(t)|$ reaches a maximum of $\Delta T_m = 42$ °C at $t_{H1} \sim 9.5$ min. Also, FEM simulations of sample H2 yielded $\overline{|\Delta T|} = (44 \pm 3)$°C and $\Delta T_m = 50$ °C at $t_{H2} \sim 16.7$ min. We have also found that $\Delta T_m = 38$ °C at $t_{G1} \sim 5.4$ min, and $\overline{|\Delta T|} = (34.5 \pm 1.6)$°C in sample G1.

On the other hand, Fig. 3(b) displays the radial temperature profiles at $z=0$ for samples H1, H2, and G1 calculated at t_{H1}, t_{H2}, and t_{G1}, respectively (see Fig. 3(a)). Regardless the material used in plungers/die, the results clearly demonstrated that the temperature is not homogeneous within the sample/die region. Inside the samples, the temperature gradient along the radial direction was found to be close to 3%. Additionally, the difference in temperature between the center of the samples and T_D were found to be 75 (H1), 70 (H2), and 60 °C (G1).

The next step is to inspect the influence of the above sintering conditions on the phase content of the consolidated samples. We first mention that the optimum sintering temperature for producing nearly single-phase Bi-2223 is $T_s \sim 845$ °C [16]. Also, samples obtained at temperatures below or above T_s usually exhibit extra phases as Ca_2PbO_4, Bi-2201, and Bi-2212 [17,18]. Accordingly, Fig. 4 shows the X-ray diffraction patterns taken from powders of the pristine material and samples H1, H2, and G1. Powders of the last three samples were obtained after crushing the SPS pellets. For comparison reasons, the XRD pattern of the pre-reacted Bi-2223 powder, termed pristine powder, is displayed in Fig. 4(a) and reveals that most of the indexed reflections are related to the high-T_c Bi-2223 phase. We have also found similar patterns in samples H1 and G1. However, the results also indicate that most of the intense peaks in the pattern of sample H2 belong to the Bi-2212 phase. At first approximation, by considering that all samples are comprised of only two phases (Bi-2223 and Bi-2212), then a roughly estimate of the volume fraction of the $Bi_2Sr_2CaCu_2O_{8+\delta}$ (Bi-2212) phase yields ~3, 6, 60, and 5% in the pristine powder and samples H1, H2, and G1, respectively. The presence of traces of the Bi-2212 phase in the X-ray pattern of consolidated $Bi_{1.65}Pb_{0.35}Sr_2Ca_2Cu_3O_{10+\delta}$ samples by SPS is an expected result, as reported elsewhere [4,19]. However, the above results indicate that the volume fraction of the Bi-2223 phase in sample H2 has been altered significantly after the SPS consolidation. Such a large amount, close to 60%, of the Bi-

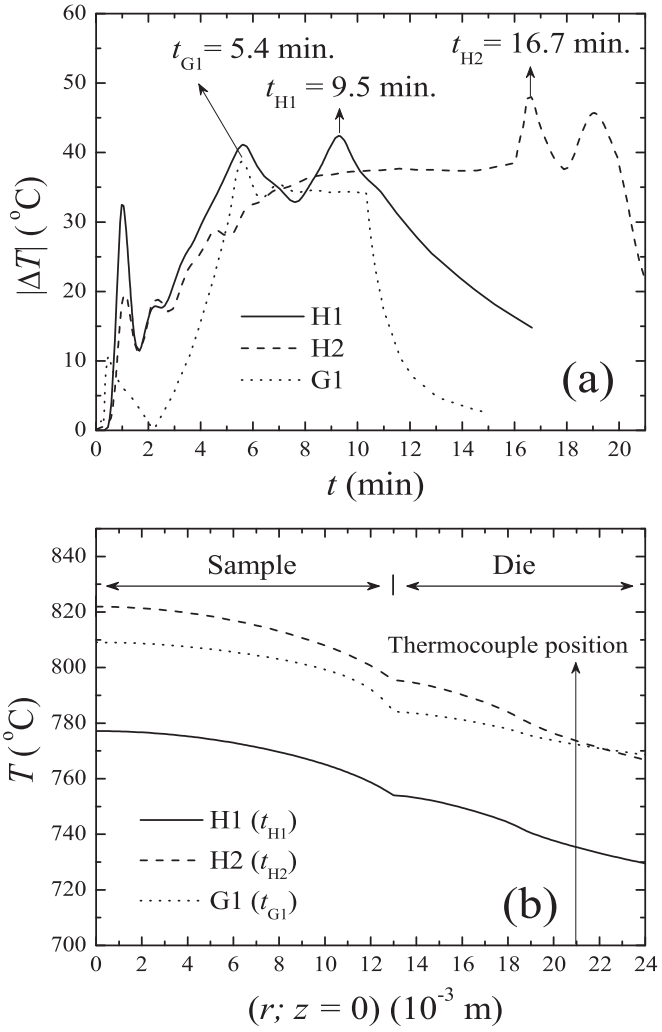

Fig. 3. (a) Estimated temperature difference during the SPS process for the studied samples; (b) the simulated radial temperature profiles for $z=0$ of samples H1, H2, and G1, respectively (see text for details).

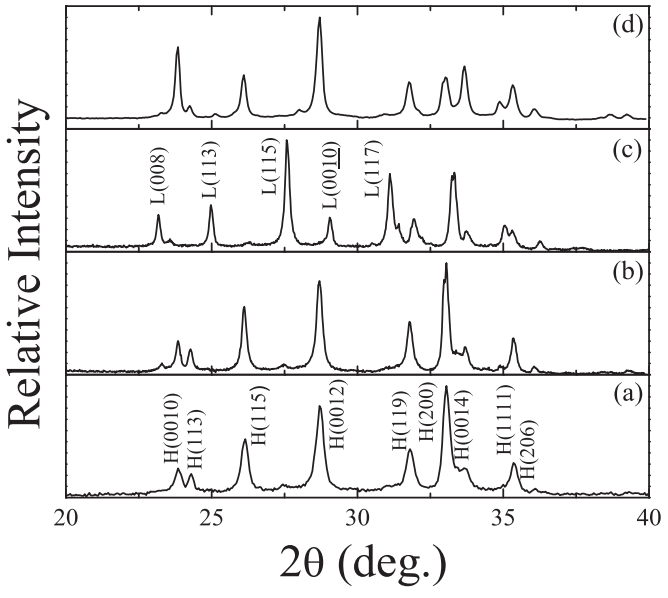

Fig. 4. X-ray diffraction patterns taken from the pre-reacted Bi-2223 powder (pristine powder) (a), and powders obtained after crushing the SPS pellets H1 (b), H2 (c), and G1 (d). The reflections belonging to the Bi-2223 (H(*hkl*)) and Bi-2212 (L(*hkl*)) phases are marked by Miller indexes in (a) and (c), respectively.

2212 phase indicates that appreciable volume fraction of the starting Bi-2223 phase has been converted during the SPS process. This result is somewhat unexpected due to the fact that all samples were consolidated from the same starting Bi-2223 powder. Taking into account the preparation conditions described in Section 2, the two different parameters used for consolidation of samples H1 and H2, obtained by using the all-steel setup, must be considered: (i) the consolidation temperature; and (ii) the heating time (see Table 1). A careful analysis of the results, however, indicates that the former parameter may be disregarded based on the fact that sample G1 was consolidated at the same temperature and its phase composition remained essentially unaltered. The second parameter to be addressed is then the heating rate used during the SPS process. The effect of the heating rate on the consolidation process of samples H1, H2, and G1 may be related to the temperature profiles displayed in Fig. 2. Here, it is important to point out that the shape of the temperature profile is strongly dependent on the properties of the material used in the plungers/sample/die setup. Heating of the setup in SPS consolidation is characterized by a resistive process and the distribution of temperature along the setup is mainly determined by the thermal conductivity of the materials used [12]. Under this circumstance, the results displayed in Fig. 3(a) are of interest and indicate that, in sample H1, ΔT increases abruptly and reaches a local maximum of ~30 °C at only $t=1$ min. An estimate of the heating rate in the range $0 \le t \le 1$ min for sample H1 yields HR=250 °C/min, a value two times higher than the expected of 135 °C/min used in the experiment (see Table 1). We also mention here that, in sample G1, the obtained value of HR is ~138 °C/min, a value in line with the pre-set ratio of ~145 °C/min.

To prevent the initial overheating observed in sample H1, the value of the HR for sample H2 has been also reduced to ~50 °C/min. Under this condition, the observed temperature peak at $t=1$ min decreases to ~20 °C and the HR estimated from the temperature profile was ~165 °C/min. This result strongly indicates that in the all-steel setup the heat transfer from the plungers/die to the sample occurs at a faster rate. As a consequence and after the first 8 min, the temperature in the region where the sample is located reaches a value of ~800 °C, and remains essentially constant in the range $8 \le t \le t_D$ (see Fig. 3(a)). It is important to point out that, for sample H2, the temperature in the sample region was higher than T_D over 12 min. Thus, it is reasonable to assure that to subject samples to a prolonged time at higher temperatures promotes the formation of the 2212 phase. Notice that in samples H1 and G1 a consolidation time of 5 min is enough for increasing the volume fraction of the Bi-2212 phase from 3 to 6%.

On the other hand, it is expected that all the above results have their counterpart on the magnetic and transport properties of the obtained samples. Following this discussion, the temperature dependence of the magnetization measured under zero-field cooling (ZFC) and field cooling (FC) conditions, in pellets of samples H1, H2, and G1, are displayed in Fig. 5. For comparison reasons, the experimental $M(T)$ data of the pristine powder is also shown in this figure. The ZFC/FC curves provide important information regarding the shielding/pinning capabilities of the superconducting samples. In samples H1 and G1, the ZFC diamagnetic contribution decreases monotonically with increasing temperature and the diamagnetic signal vanishes at the onset intragranular critical temperature, T_{cg1} = 105 K. In contrast, the ZFC curve of sample H2 first decreases monotonically, undergoes a change in its slope close to T_{cg2}=90 K, and finally the diamagnetic signal vanishes at T_{cg1} = 105 K (see inset of Fig. 5). It is important to point out that T_{cg1} and T_{cg2} are related to the superconducting critical temperatures of phases Bi-2212 and Bi-2223, respectively. Thus, the identification of a superconducting transition associated with the

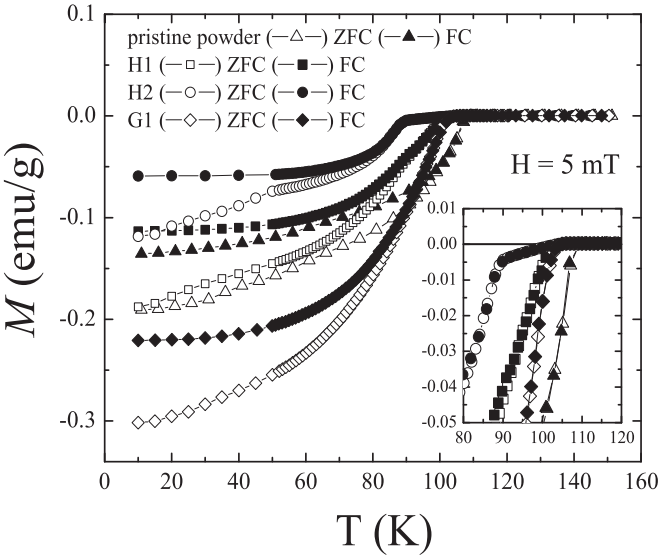

Fig. 5. Temperature dependence of ZFC/FC magnetization curves measured in the pristine powder and pellets of SPS samples H1, H2, and G1 under an applied magnetic field of 5 mT. The inset shows an expanded view of the superconducting transition region. Lines between points are guides for the eyes.

Bi-2212 phase at T_{cg2} in sample H2 is in line with the results of the XRD analysis discussed above. The magnetization measurements performed in the pristine powder revealed that the transition to the superconducting state starts at T_{cg1}=109.4 K, a value very close to the critical temperature reported for Bi-2223 single crystals [3]. This is an expected result because the pristine powder is nearly single-phase Bi-2223, as inferred from the XRD data.

Another relevant feature of the experimental $M(T)$ dependence concerns the difference between ZFC and FC curves. In powder samples such a difference is closely related to the trapped magnetic flux inside grains, a feature quite different in pellet samples that includes information arising from the shielding capability (ZFC) and flux pinning (FC) at intergranular regions of the material [20]. It is extremely curious that the qualitative behavior of experimental $M(T)$ curves measured in pellet samples is very similar to that observed in the pristine powder. Such a result strongly suggests that the intergranular coupling in SPS samples is very weak. In line with this observation, we have defined the difference $\Delta M = M_{FC}(10\text{ K}) - M_{ZFC}(10\text{ K})$ to evaluate the strength of the intergranular properties of these samples [16]. Values of ΔM were found to be $\Delta M_{H1} \sim 0.07$, $\Delta M_{H2} \sim 0.06$, $\Delta M_{G1} \sim 0.08$, and $\Delta M_{powder} \sim 0.06$ emu/g. The results indicate that $\Delta M_{pellets} \approx \Delta M_{powder}$ for all samples, further indicating that the intergranular contribution to $M(T)$ data in pellet samples is essentially negligible and that the diamagnetic contribution arises mostly from the superconducting grains. Also, these findings point out to the formation of grains with shell-core morphology during the SPS consolidation, as reported previously [4]. In fact, assuming that the shell of the superconducting grains is oxygen deficient, the magnetic response of pellets is likely to be similar to those from isolated grains (i.e., like a powder sample), as observed in the $M(T)$ data. A procedure to restore, at least partially, the oxygen content along grain boundaries of the samples is to subject the materials to a post-annealing heat treatment, as discussed below [4,5].

Fig. 6 shows the temperature dependence of the magnetization, $M(T)$, measured in post-annealed samples referred to as H1+O_2, H2+O_2, and G1+O_2. Besides the higher diamagnetic contribution of the annealed samples, the quantitative and qualitative behavior of the ZFC/FC curves are quite different from those displayed in Fig. 5. In this case, estimated values of ΔM yields 0.35 and 0.36 for samples H1+O2, H2+O2, respectively, and 0.6 for the sample

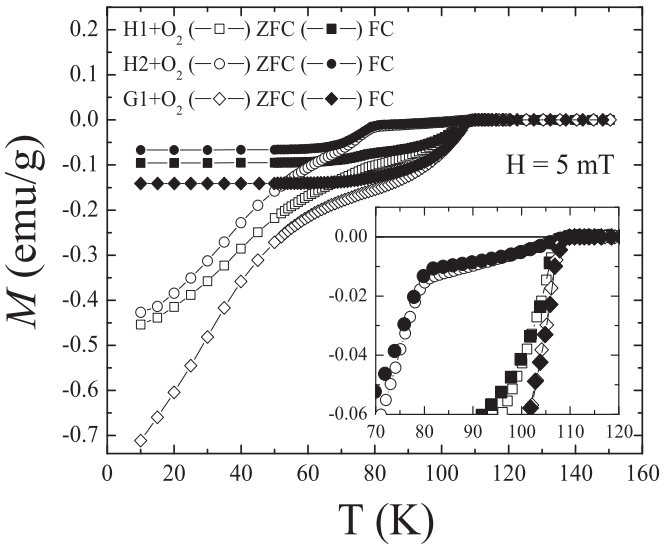

Fig. 6. ZFC/FC magnetization curves as a function of temperature measured in post-annealed samples H1, H2, and G1 under an applied magnetic field of 5 mT. The inset shows an expanded view of the superconducting transition region. Lines between points are guide for the eyes.

G1 + O2, a value rather low and close to only ~40% when compared with other samples. These results give additional support to the use of the all-graphite setup instead the all-steel device for SPS consolidation of Bi-2223 ceramic superconductors. We mention here that values of T_{cg1} close to 110 K were observed in all samples provided that they were subjected to the post-annealing heat treatment. As far as this point is concerned, a careful inspection of the inset of Fig. 6 indicates that the decrease of T_{cg2} from 90 to 80 K, in sample H2 + O2, a feature related to the increase in the oxygen content of the $Bi_2Sr_2CaCu_2O_{8+\delta}$ (Bi-2212) phase, which has its superconducting transition temperature varied from 90–60 K when $\delta > 0.2$, as reported elsewhere [21]. This experimental result supports the idea that the Bi-2212 phase seems to be a good candidate for synthesis by using the SPS technique, a study that requires further investigation.

5. Conclusions

In summary, the effect of plungers/die built with different materials on the superconducting properties of Bi-2223 ceramic consolidated by using the spark plasma sintering SPS technique has been investigated. Experimental temperature profiles obtained during the SPS consolidation were fitted to the generated curves from a finite element simulation model integrated with a PID control. The comparison of the experimental and theoretical curves demonstrated the good accuracy of the proposed model, providing more insights into the temperature evolution within the sample. The obtained results indicate that samples consolidated by using the all-graphite setup display higher superconducting volume fraction of the Bi-2223 phase when compared to those consolidated with the all-steel setup. By the virtue of the SPS method to be conducted under vacuum, we have also found that the SPS samples are comprised of grains with a shell-core morphology in which the shell is oxygen deficient. The results also indicate that the carbon of the mold has no influence on promoting the oxygen deficiency of the shell layer. Further strategies must be tested in order to avoid this undesired result mostly due to the fact that the SPS consolidation is conducted under vacuum. Finally, even though the SPS samples obtained by using tool steel dies were found to have lower superconducting volume fraction, the use of this setup raises the possibility to achieve higher values of uniaxial compacting pressure during the process.

Acknowledgments

The authors acknowledge financial support from Brazil's Agencies CAPES, FAPESP (Grants nos. 2013/07296-2 and 2014/19245-6), and CNPq (Grants nos. 306006/2015-4 and 444712/2014-3), and Petrobras company.

References

[1] R. Orrù, R. Licheri, A.M. Locci, A. Cincotti, G. Cao, Consolidation/synthesis of materials by electric current activated/assisted sintering, Mater. Sci. Eng. B 63 (2009) 127–287.
[2] U. Anselmi-Tamburini, S. Gennari, J.E. Garay, Z.A. Munir, Fundamental investigations on the spark plasma sintering/synthesis process: II. modeling of current and temperature distributions, Mater. Sci. Eng. A 394 (2005) 139–148.
[3] T. Fujii, T. Watanabe, A. Matsuda, Comparative study of transport properties of $Bi_2Sr_2Ca_2Cu_3O_{10+\delta}$ and $Bi_2Sr_2CaCu_2O_{8+\delta}$ single crystals, Physica C. 357–360 (2001) 173–176.
[4] E. Govea-Alcaide, I.F. Machado, M. Bertolete-Carneiro, P. Muné, R.F. Jardim, Consolidation of Bi-2223 superconducting powders by spark plasma, J. Appl. Phys. 112 (2012) 113906–113914.
[5] E. Govea-Alcaide, I.F. Machado, R.F. Jardim, 10 to 25-fold increase in the transport superconducting critical current density of spark-plasma sintered Bi-2223 superconductors, J. Appl. Phys. 117 (2015) 043903–043908.
[6] Y. Gao, Y.J. Wu, X.M. Chen, J.P. Cheng, Y.Q. Lin, Y. Ma, Dense YMn2O5 ceramics prepared by spark plasma sintering, J. Am. Ceram. Soc. 91 (2008) 3728–3730.
[7] R. Mazumder, D. Chakravarty, D. Bhattacharya, A. Sen, Spark plasma sintering of $BiFeO_3$, Mater. Res. Bull. 44 (2009) 555–559.
[8] K. Zehani, F. Mazaleyrat, V. Loyau, E. Laboure, Effect of temperature and time on properties of spark plasma sintered NiCuZn: Co ferrite, J. Appl. Phys. 109 (2011), 07A504-07A507.
[9] N. Chennoufi, G. Majkic, Y.C. Chen, K. Salama, Temperature, current, and heat loss distributions in reduced electrothermal loss spark plasma sintering, Metal. Mater. Trans. A 40A (2009) 2401–2409.
[10] S. Ovtar, S. Gallet, L. Minier, N. Millot, D. Lisjak, Control of barium ferrite decomposition during spark plasma sintering: towards nanostructured samples with anisotropic magnetic properties, J. Eur. Ceram. Soc. 34 (2014) 337–346.
[11] A.J. Mackie, G.D. Hatton, H.G.C. Hamilton, J.S. Dean, R. Goodall, Carbon uptake and distribution in Spark Plasma Sintering (SPS) processed $Sm(Co, Fe, Cu, Zr)_z$, Mater. Lett. 171 (2016) 14–17.
[12] S. Muñoz, U. Anselmi-Tamburini, Temperature and stress fields evolution during spark plasma sintering processes, J. Mater. Sci. 45 (2010) 6528–6539.
[13] C. Wang, L. Cheng, Z. Zhao, FEM analysis of the temperature and stress distribution in spark plasma sintering: modelling and experimental validation, Comp. Mater. Sci. 49 (2010) 351–362.
[15] J. Ziegler, N. Nichols, Optimum settings for automatic controllers, Trans. ASME 64 (1942) 759–765.
[16] P. Muné, E. Govea-Alcaide, R.F. Jardim, Influence of the compacting pressure on the dependence of the critical current with magnetic field in polycrystalline $(Bi\text{-}Pb)_2Sr_2Ca_2Cu_3O_x$ superconductors, Physica C 384 (2003) 491–500.
[17] D. Pandey, A.K. Singh, P.K. Srivastava, A.P. Singh, S.S.R. Inbanathan, G. Singh, Towards the rapid synthesis of pure 2223 powders with $Bi_{2_x}Pb_xSr_2Ca_2Cu_3O_y$ compositions by semi-wet methods II. Optimization of Pb content using Pb-Sr-Ca carbonate precursors, Physica C 241 (1995) 279–291.
[18] P. Majewski, Phase diagram studies in the system Bi-Pb-Sr-Ca-Cu-O-Ag, Supercond. Sci. Technol. 10 (1997) 453–467.
[19] P. Badica, G. Aldica, J.R. Groza, M.-C. Bunescu, S. Mandache, Reactive-field-assisted-sintering of freeze-dried powders in the BSCCO system, Supercond. Sci. Technol. 15 (2002) 32–42.
[20] F. Pérez, X. Obradors, J. Fontcuberta, X. Bozec, A. Fert, Magnetic flux penetration and creep in a ceramic $(Y,Sm)Ba_2Cu_3O_7$ superconductor, Supercond. Sci. Technol. 9 (1996) 161–175.
[21] T. Watanabe, T. Fujii, A. Matsuda, Pseudogap in $Bi_2Sr_2CaCu_2O_{8+\delta}$ studied by measuring anisotropic susceptibilities and out-of-Plane transport, Phys. Rev. Lett. 84 (2000) 5848–5851.